Journal of Applied Polymer Science

Molecular dynamics simulations of molecularly imprinted polymer approaches to the preparation of selective materials to remove norfloxacin

Yu Kong,[1] Ningwei Wang,[2] Xiaoni Ni,[3] Qiyi Yu,[1] Hong Liu,[4] Weihong Huang,[1] Wanzhen Xu[1]

[1]School of Environment and Safety Engineering, Jiangsu University, Zhenjiang 212013, People's Republic of China
[2]Zhenjiang Entry-Exit Inspection Quarantine Bureau, Zhenjiang 212008, People's Republic of China
[3]Zhenjiang Institute for Drug Control of Jiangsu Province, Zhenjiang 212003, People's Republic of China
[4]Institute of Theoretical Chemistry, State Key Laboratory of Theoretical and Computational Chemistry, Jilin University, Changchun 130023, People's Republic of China
Correspondence to: W. Huang (E-mail: whuang630@ujs.edu.cn) and W. Xu (E-mail: xwz09@ujs.edu.cn)

ABSTRACT: A novel molecularly imprinted polymer (MIP) designed by molecular dynamics (MD) simulations was successfully prepared with norfloxacin as a template molecule, methyl acrylic acid as a functional monomer, and ethylene glycol dimethacrylate as a crosslinker. According to the theoretical prediction and experimental preparation methods, three kinds of molecular imprinting materials were designed and synthesized with MD simulations and molecular imprinting technology. The best ratio of the template to the functional monomer to the crosslinker was 1:8:40 in these studies. The experimental results illustrate that the MD simulations were credible in compounding the components of the MIPs. The structure of the prepared polymers were characterized with various methods. To analyze the adsorption performances, many kinds of static adsorption tests, including kinetic, isotherm, and selectivity tests, were used. The results indicate that the novel adsorbents conformed to the pseudo–second-order kinetic equation and followed the Langmuir isotherm model. The adsorption amounts of MIP2 at a ratio of 1:8:40 were about 29.35 mg/g at 298 K. The selective adsorption and reusable performance of norfloxacin were excellent. © 2015 Wiley Periodicals, Inc. J. Appl. Polym. Sci. **2016**, *133*, 42817.

KEYWORDS: adsorption; functionalization of polymers; molding; molecular recognition; properties and characterization

Received 23 March 2015; accepted 5 August 2015
DOI: 10.1002/app.42817

INTRODUCTION

Fluoroquinolones (FQs) are synthetic antibacterial drugs that are commonly used for the prevention and control of human and animal disease caused by several bacterial agents.[1,2] Their potential problems are that FQs can residue in animals and can also discharge into the environment by animal urine or other ways. The use of FQs have increased in recent years, and among them, norfloxacin (NOR) has been the most commonly used in the world. The wide application of NOR in food-producing animals has caused concerns about the residues present in foods of animal origin; these residues can cause pathogenic resistance, nausea, vomiting, anaphylactic reactions, and even neurological symptoms in humans.[3–8] What is more, it can lead to joint pain and swelling in children. Meanwhile, the European Union has established that the maximum residue limits for FQs in animal products must be less than 100 g/kg.[9] So, it is necessary for us to separate and detect FQs with a sensitive and selective method to ensure that food is kept far away from antibiotic residues.

At present, several analytical methods for removing and determining FQ residues in food and environment have been set up; these use different extraction procedure and clean-up conditions. The traditional treatments of NOR include advanced chemical oxidation, coagulation, and flocculation methods, the sand filter method, membrane treatment technology, the activated sludge method, and ultrasonic and artificial wetlands.[10] However, these methods' shortcomings include a lack of specific recognition in the adsorption process, although their adsorption performances are good. In this case, these conventional methods of adsorption may remove other valuable compounds more or less in the adsorption of NOR. Therefore, the development of a method for removing this target from the environment has become mandatory in recent years.

Additional Supporting Information may be found in the online version of this article.

Molecular imprinting technology is well known for the formation of specific recognition sites with memory of the functional groups of a template.[11] As a solution, molecularly imprinted polymers (MIPs) are used as novel selective synthetic sorbents, which are based on the combination of functional monomers with crosslinkers in the presence of the template molecules and then the removal of the templates to leave the recognition sites consistent with the template structure.[12,13] Compared with classical adsorbents, MIPs exhibit favorable molecular recognition capability and stability and a high selectivity toward the target object. The advantages of MIPs have led to the development of MIP applications, including liquid chromatography,[14] solid-phase extraction,[15] and senors.[16] During recent years, a series of FQs–MIPs have been used to detect and separate FQs from complex media; these include the determination of FQ residue in soil samples,[17] animal tissues and eggs,[18,19] milk,[20–22] muscle, and plasma.[23,24] Ciprofloxacin MIPs were successfully prepared and used as a selective sorbent to detect FQs in soil samples; these MIPs were synthesized by different functional monomers and solvents.[25] An enrofloxacin MIP was prepared for the specific selective extraction of ciprofloxacin and enrofloxacin from tissue and urine samples.[26] Ofloxacin (OFL) MIPs were also prepared to detect six FQs from human serum samples at the same time.[27]

In previous studies, there have been few reports on the study of the mechanisms occurring in the prepolymerization in the process of molecular imprinting.[28] Recently, Henthorn and Peppas[29] discussed the influence of the crosslinking density on MIPs' recognition results through the simulation of the prepolymerization process. As we all know, the interaction between templates and functional monomers is the key to molecular imprinting technique. Thus, the selection of the ideal ratio between the template and functional monomer is essential. However, this method has some shortcomings; these include a long experimental period and so on. So, molecular dynamics (MD) simulations are used to rationally design a molecularly imprinted system and analyze the mechanism at the molecular level, but few studies have focused on discussing the relationship between template and the ideal monomer.[30–33]

In this study, by combining the method of the molecular imprinting technique and MD simulations, we designed and prepared MIPs to adsorb and separate NOR specifically. In addition, this method could greatly improve the efficiency of the preparation of molecularly imprinted materials with MD simulation, and it could also reduce the material cost and shorten the experimental time. What is more important, the introduction of MD simulation is helpful for exploring and analyzing the molecular imprinting recognition mechanism of the molecular imprinting process in the prepolymerization system. It also has vital theoretical guiding significance for the rational design and synthesis of molecularly imprinted materials that can be used for the selective separation of environmental pollutants. On the basis of the simulation results, three kinds of MIPs were prepared as adsorbents, which were synthesized with different ratios of template molecules (NOR) to functional monomers [methyl acrylic acid (MAA)] to crosslinkers [ethylene glycol dimethacrylate (EGDMA)]. Then, the structures of the MIPs were examined, and the adsorption performances were analyzed. After that, we determined the best one of the three that could selectively recognize NOR.

EXPERIMENTAL

Chemicals and Instruments

NOR, OFL, sulfamethoxazole (SMZ), MAA, EGDMA (98%), azobisisobutyronitrile (AIBN; 99%), and triethylamine were purchased from Aladdin Reagent Co. (Shanghai, China). Methanol [analytical reagent (AR)], ethanol (AR), acetic acid (AR), acetonitrile (ACN), and activated charcoal granular (AR) were supplied by Sinopharm Chemical Reagent. All of these chemicals and solvents were used without further purification.

A Shimadzu LC-2010A HPLC system equipped with an ultraviolet detector (Shimadzu, Japan) was used to determine the concentration of NOR in solution. All of the separations were carried out on a Waters C18 column (150 × 4.6 mm^2, 5 m). The mobile phase consisted of 0.05 mol/L phosphate buffer (the pH was adjusted to 2.4 with triethylamine) and ACN (80 : 20 v/v) and was filtered by a microporous membrane. The filtration rate was 1.0 mL/min, and the detection wavelength was set at 280 nm. The column temperature was 30°C, and the injection volume was 20 μL.

A Tristar II 3020 instrument was used to measure the specific area (in square meters per gram), pore volume (in cubic centimeters per gram), and pore diameter (in nanometers) of the prepared nanoparticles. The S-4800 field emission scanning electron microscope that we used was obtained from Hitachi. The Nicolet Nexus 470 Fourier transform infrared spectrometer that we used was obtained from Thermoelectrics.

MD Simulations

All-atom MD simulations were performed with the Materials Studio 7.0 Windows software package (Accelrys, San Diego, CA). All of the studied molecular systems and the construction and simulation procession of the prepolymerization system were made and parametrized with a Condensed-phase Optimized Molecular Potential for Atomistic Simulation Studies (COMPASS) field. Before the molecular simulations of the prepolymerization process, MD were examined on the preliminary optimization of the molecular structure and energy of NOR, MAA, EGDMA, and ACN, respectively. The optimization process used a COMPASS field in a discover module, and the previous molecules were energy-minimized with 5000 steepest descent and 5000 conjugate gradient steps to remove bad contacts. After these optimization procedures, we built three virtual boxes at a temperature of 298 K according to the ratios in Table I, which continued to be energy-minimized, as in the previous operation. To ensure that the energy of the prepolymerization system stayed at a stable and relatively equilibrium state, we needed to perform an MD simulation of the prepolymerization system. First, the prepolymerization system was equilibrated during a 200-ps time under conditions of cannonical ensemble at a temperature of 298 K. Then, the systems were heated to 698 K and at equilibrium, again at a high temperature, with the same simulation conditions as used previously. This step was performed to allow the prepolymerization system to cross over the energy barriers. Next, the temperature was reduced to 298 K

Table I. Composition of the Simulated MIP Prepolymerization Mixtures

Polymer	NOR (mmol)	MAA (mmol)	EGDMA (mmol)	ACN (mmol)	Molar ratio
MIP1	1	4	20	173	1:4:20
MIP2	1	8	40	173	1:8:40
MIP3	1	12	60	173	1:12:60

and equilibrium again. After the operations, a simulated annealing process was initiated. This involved all of the components in the system and was followed by a heating step (up to 698 K) and then gradual cooling at in 10,000 steps with the annealing instructions in the Forcite module under conditions of cannonical ensemble. Finally, we continued to equilibrate the system under conditions of 298 K and 0.0001 GPa with an NPT ensemble. The calculation of nonbonded interactions had a 10-Å cutoff.

Radial distribution functions (RDFs) were performed to determine and analyze the structural characteristics of the prepolymerization system and the distribution of functional monomers around the NOR molecule. Here, RDF [or $g(r)$] is defined as the ratio between the observed number densities, and it was derived from the Material Studio software directly.

Preparation of the Imprinted Polymers and Nonimprinted Polymers (NIPs)

The NOR MIPs were prepared with different ratios of components, and the composition of the prepolymerization mixtures are presented in Table II. All these polymers were prepared by thermally initiated polymerization within a 20-mL thick-walled glass tube. NOR (1 mmol) and MAA (4, 8, 12 mmol) were dispersed in ACN (9 mL) with stirring for 2 h in an ice bath for prepolymerization, and then, EGDMA (20, 40, 60 mmol) as a crosslinker and 0.25 mmol of AIBN as an initiator were successively added to the previous solution. Then, the solution was sonicated for 10 min and purged with nitrogen gas for 10 min to remove oxygen before the glass tube was sealed. Next, the tube was placed in a water bath at 60°C for 24 h under nitrogen protection with stirring. At the end of the period, the mixture showed a milky suspension. After polymerization, the obtained polymer particles were filtered and washed with ethanol and distilled water, respectively, three times and then dried *in vacuo*. Finally, we put the particles into a column, washed them with methanol–acetic acid (9 : 1 v/v) to remove the template molecules, and dried them *in vacuo*. The NIPs were prepared in an identical manner but in the absence of template molecules. The synthetic process is shown in Figure 1.

Adsorption Experiments

All of the following adsorption experiments, including adsorption isotherm, kinetic, and selectivity tests, were used to investigate the adsorption properties and the specific adsorption capacity of the MIPs and NIPs.

Adsorption Kinetic Studies. For adsorption kinetic studies, MIPs (or NIPs, 10 mg) were suspended in a batch of centrifuge tubes containing NOR aqueous solution (7 mL, 50 mg/L). The centrifuge tubes were shaken in a vapor-bathing, constant-temperature vibrator at a preset temperature of 298 K. Then, these centrifuge tubes were taken out successively at defined times (10, 20, 30, 60, 90, 120, 150, 180, 210, 240, 270, and 300 min) and then centrifuged at 8000 rpm. The residual concentrations of NOR were measured with the HPLC method, and the adsorbed amount of NOR at time t was obtained with the following equation:

$$q_t = (C_0 - C_t)V/m \quad (1)$$

where q_t is the adsorption capacity of the MIPs (or NIPs) at time t (mg/g); C_0 and C_t are the initial concentration of the NOR aqueous solution and the concentration of the NOR aqueous solution at time t (mg/L), respectively; V is the volume of the NOR aqueous solution (mL); and m is the mass of the NOR MIPs (NIPs; mg).

Adsorption Isotherm Studies. For adsorption isotherm studies, the MIPs (or NIPs, 10 mg) were added to 10 centrifuge tubes, each containing 7 mL of NOR aqueous solution with concentration gradients from 10 to 100 mg/L. The mixtures were shaken in a vapor-bathing, constant-temperature vibrator at a preset temperature of 298 K. When the adsorption equilibrium time (3 h) was reached, we then took all of the centrifuge tubes out and centrifuged them at 8000 rpm. The supernatant was used to determine the concentration of the NOR solution with the

Table II. Materials Synthesized in This Study

Polymer	NOR (mmol)	MAA (mmol)	EGDMA (mmol)	AIBN (mmol)	ACN (mmol)
MIP1	1	4	20	0.25	173
NIP1	0	4	20	0.25	173
MIP2	1	8	40	0.25	173
NIP2	0	8	40	0.25	173
MIP3	1	12	60	0.25	173
NIP3	0	12	60	0.25	173

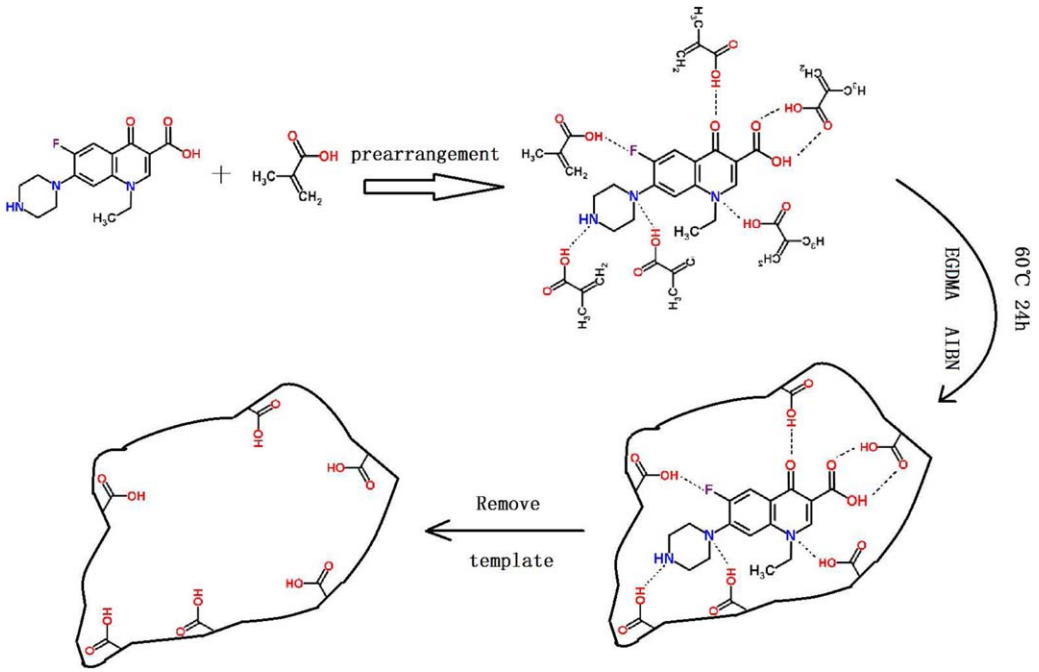

Figure 1. Schematic for the preparation of the NOR MIPs. [Color figure can be viewed in the online issue, which is available at wileyonlinelibrary.com.]

HPLC method, and the adsorption capacity was calculated according to the following equation:

$$q_e = (C_0 - C_e)V/m \quad (2)$$

where q_e is the adsorption capacity of the MIPs (or NIPs; mg/g) and C_e (mg/L) is the concentration of the final NOR solution.

Adsorption Selectivity and Competitiveness Studies. First, 7-mL solutions containing 50 mg/L NOR, OFL, or SMZ were prepared, and 10 mg of MIP2 (or NIP2, where the number after MIP and NIP represents experiments with different situations) was added to each. Second, 10 mg of MIP2 was added to the three-component mixtures containing 50 mg/L each of NOR, OFL, and SMZ. The following operations were similar to the adsorption isotherms. To highlight the adsorption performance of MIP2, we used granular activated charcoal to adsorb the targets in solution, and the operation method was the same as that used for MIP2. The temperature was set at 298 K for 3 h. The structures of NOR, OFL, and SMZ are shown in Figure 2. The selectivity and competitiveness of MIP were obtained with the following equations [eqs. (3)–(5)]:

$$K_d = q_e/C_e \quad (3)$$

where K_d is the distribution coefficient (L/g):

$$k = K_d(\mathrm{NOR})/K_d(\mathrm{R}) \quad (4)$$

where k is the selectivity coefficient and R represents a competitive compound, such as OFL or SMZ:

$$k\prime = k_{\mathrm{MIPs}}/k_{\mathrm{NIPs}} \quad (5)$$

where k' is the relative selectivity coefficient.

RESULTS AND DISCUSSION

MD Treatments

In this section, the close degrees of NOR to MAA are discussed from the standpoint of RDF. In Figure 3, the atoms that could form recognition imprinting sites are labeled.[14,34]

The following figures show the RDFs of atoms that could form imprinting sites. This was helpful for predicting the conditions of the MAA molecules around NOR molecules. As shown in Figure 4, TN (atom N labeled in NOR (norfloxacin) in figure 3)–MH (atom N labeled in NOR (norfloxacin) in figure 3) atomic contact was present, the interaction of TN and TF of NOR with MH of MAA. Within 3 Å, there were only TN2 (the number after "TN" represents different atom N labled in NOR) and TF (atom F labeled in norfloxacin in figure 3) atoms of MIP3 with peaks of 5.4 and 3.7.[35] In terms of these two interactions, we predicted that TN2 and TF were the main interactions with MH of MAA. The interactions between TN of NOR and MH of MAA of MIP3

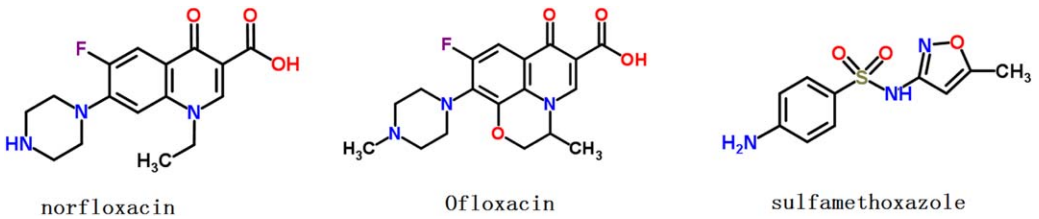

Figure 2. Chemical structures of NOR, OFL, and SMZ. [Color figure can be viewed in the online issue, which is available at wileyonlinelibrary.com.]

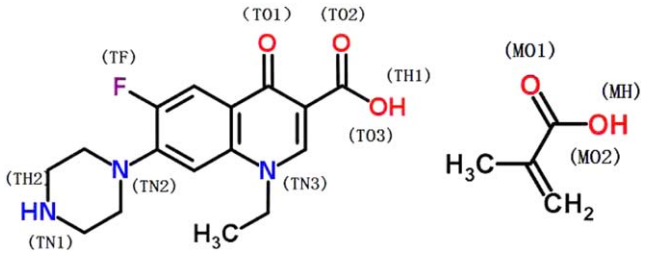

Figure 3. Chemical structures of NOR and MAA and atoms studied with RDFs. [Color figure can be viewed in the online issue, which is available at wileyonlinelibrary.com.]

were the weakest, and that with MIP2 was weaker than that with MIP1.

As shown in Figure 5, the peak value of TO1 (atom O labeled in NOR in figure 3)'–MH of MIP2 was about 40, and this was far higher than those of MIP1 and MIP3. When the distance was more than 3 Å, there were no interactions between TO1 (the number after "TO" represents different atom O in NOR) of NOR and MH of MAA. As shown in Figure 5(b), the analysis was nearly the same as discussed previously, and the peak value was about 12. As shown in Figure 5(c), when the distance between TO3 and MH was closer, the peak value of MIP2 was higher than those of the other two. This indicated that the interactions of MIP2 between the TO atoms and MH were stronger.

Figure 6 shows the interactions between TH (atom H labled in NOR in figure 3) of NOR and MO (atom O labled in MAA in figure 3) of MAA. In Figure 6(a,b), we could hardly determine which one, between MO1 and MO2, interacted with TH1 (the number after "TH" represents different atom H labled in NOR) of NOR more strongly. As shown in Figure 6(c,d), the peak of TH2–MO1 (the number after "MO" represents different atom O labled in MAA) appeared at a closer distance, and the value was higher.

In conclusion, it was not hard to see that the strongest action site was TO1–MH, and the distribution range was around 2 Å. The TO2–MH action site was weaker than that of TO1–MH but stronger than others. These interactions belonged to the short form and easily formed hydrogen bond at the sites. We predicted that TO–MH sites could play a dominant role in the process of imprinting identification. Although the peaks of TN–MH and TF–MH of MIP3 were higher than those of MIP2, the TO–TH sites of MIP2 were stronger. So, the adsorption capacity of MIP2 might have been bigger than those of MIP3 and MIP1. This result was consistent with the results from Tang *et al.*[36]

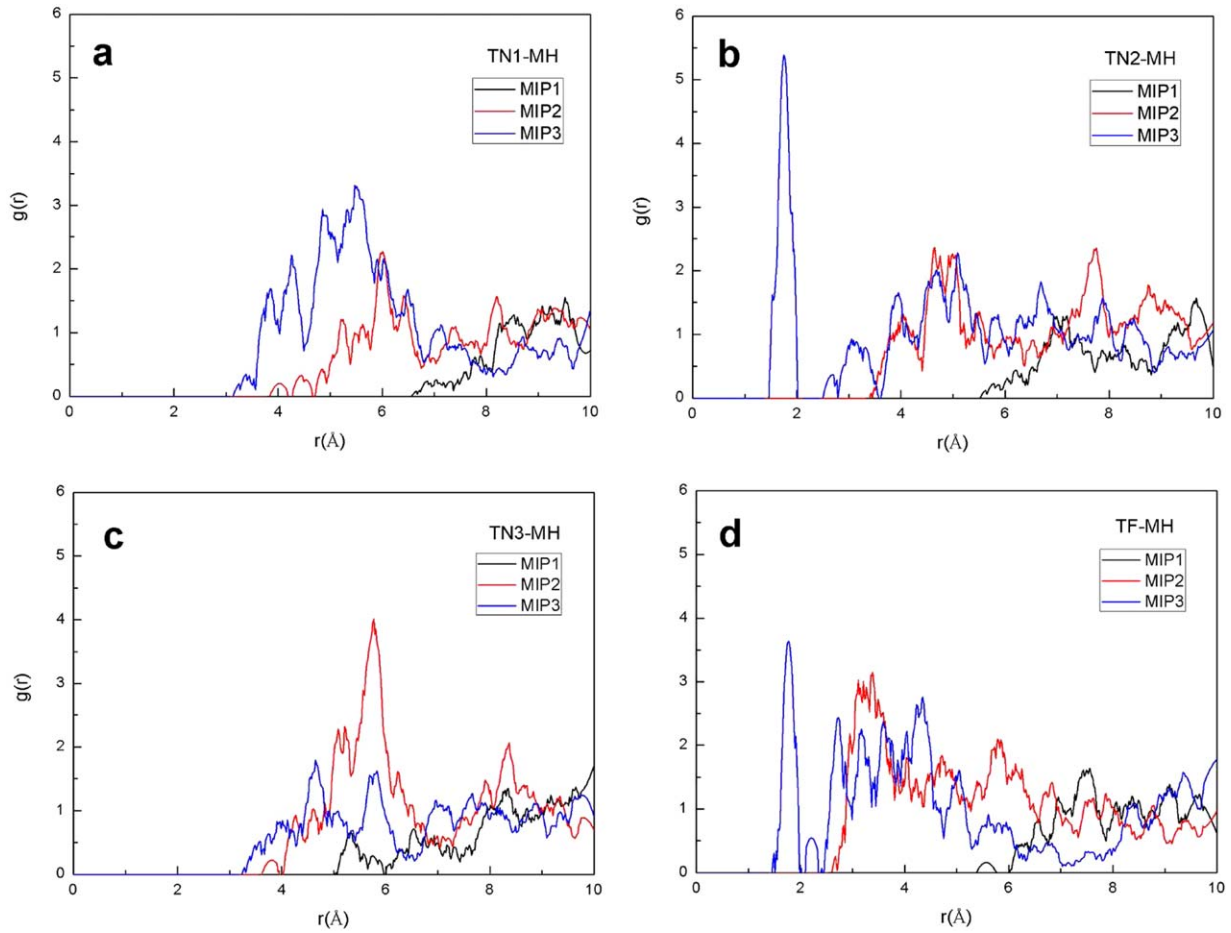

Figure 4. RDFs showing the probabilities of nitrogen and fluorine atoms of NOR at different separation distances from the hydrogen atom of MAA. r is a certain distance from a solute atom and the average bulk atom. [Color figure can be viewed in the online issue, which is available at wileyonlinelibrary.com.]

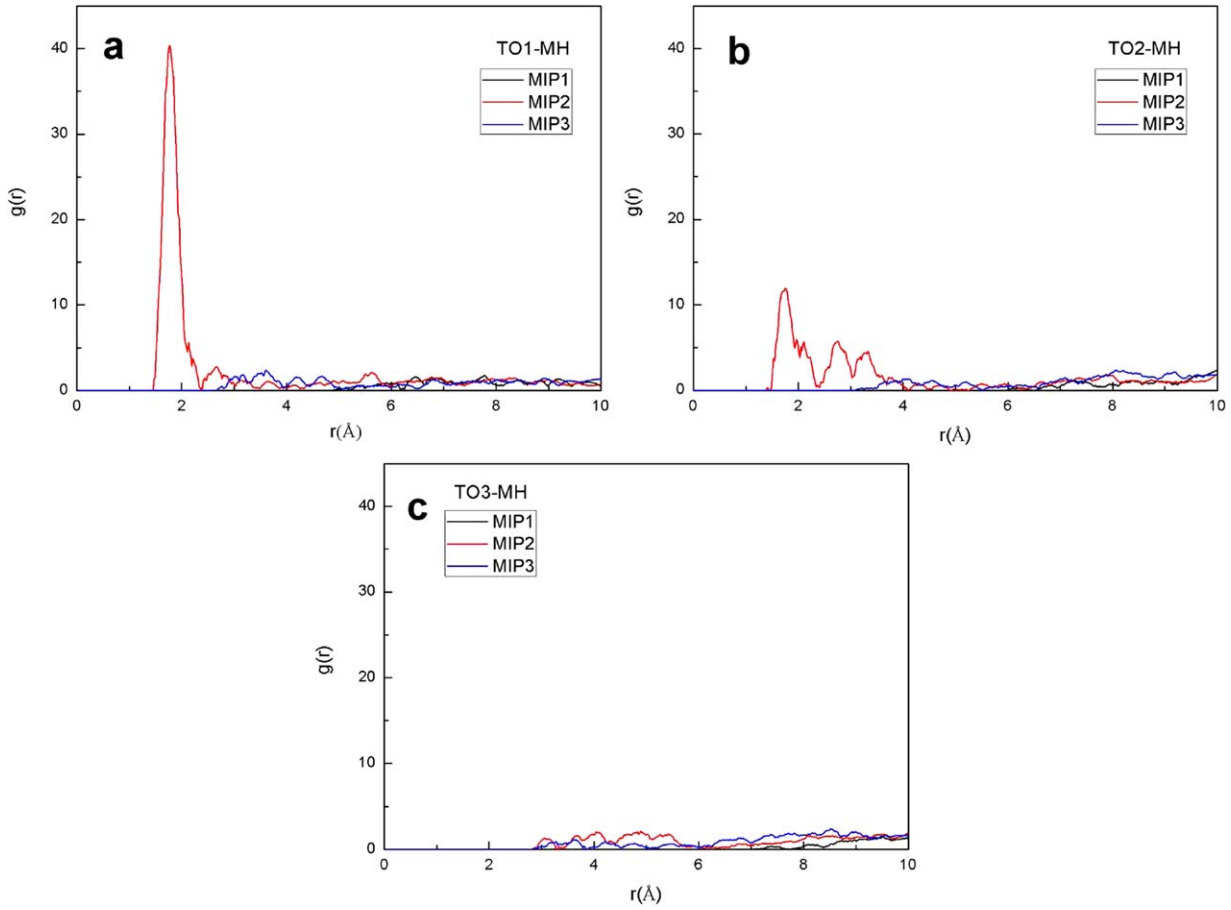

Figure 5. RDFs showing the probabilities of oxygen atoms of NOR at different separation distances from the hydrogen atom of MAA. *r* is a certain distance from a solute atom and the average bulk atom. [Color figure can be viewed in the online issue, which is available at wileyonlinelibrary.com.]

Characterization

Nitrogen Adsorption Analysis. The specific area, pore volume, and pore diameter values of the MIP2 and NIP2 particles were calculated by the Brunauer–Emmett–Teller equation and the Barrett–Joyer–Halendal model with single-point analysis. MIP2 was proven to have a higher specific surface area of 28.8 m^2/g than NIP2 (whose value was 11.3m^2/g). This was attributed to the cavities created by the imprinting process. The pore volume and average pore diameter values of MIP2 and NIP2 were 0.53 cm^3/g and 4.86 nm and 0.15 cm^3/g and 4.32 nm, respectively; this indicated that both were mesoporous. We expected MIP2 to show a better adsorption performance than NIP2.

Scanning Electron Microscopy Analysis. Scanning electron microscopy images of MIP2 and NIP2 are shown in Figure 7(a,b), respectively. As shown, we observed that there were larger surface areas and more pores in MIP2 than in NIP2. What is more, the surface of the MIPs was rougher than that of the NIPs, and this was helpful for MIP2 in the improvement of the adsorption ability to NOR.

IR Spectrum Analysis. As shown in Figure 8, the materials that we produced were studied by IR spectroscopy. Lines a, b, c, and d are the IR spectra of MIP2, MIP3, MIP1, and NIP2, respectively. We found that the three kinds of MIPs had similar IR spectral characteristics. This was mainly because the chemicals used in the experiment were identical except for their dosages. The adsorption peak at 3392 cm^{-1} in the figure represents the stretching vibrations of the amino group. The stretching vibration peak of the methyl or methylene group appeared at 2976 cm^{-1}, and the peak at 1729 cm^{-1} represents the C═O stretching vibrations. The vibration peaks of the formation of methyl appeared at 1457 and 1391 cm^{-1}. Additionally, the peaks appearing at 1259 and 1159 cm^{-1} represented the bending vibration peaks of the hydroxyl group and the stretching vibration peak of the C—O group, respectively.

Analysis of the Adsorption Kinetics

To study the adsorption mechanism, three models were used to fit the experimental data; these included the pseudo–first-order, pseudo–second-order,[37] and Elovich kinetics models.[38] These three equations are expressed in eqs. (6)–(8). The parameters of the fitting results are shown in Figure 9 and Table S1 (see the Supporting Information):

$$q_t = q_e[1-\exp(k_1 t)] \quad (6)$$

$$q_t = q_e{}^2 k_2 t/(1+q_e k_2 t) \quad (7)$$

$$q_t = \ln(ab)/b + \ln\ t/b \quad (8)$$

where k_1 and k_2 are the rate constants of the pseudo–first-order and pseudo–second-order kinetics models, respectively; $q_{e,exp}$ and $q_{e,cal}$ are the experimental and calculated values of binding

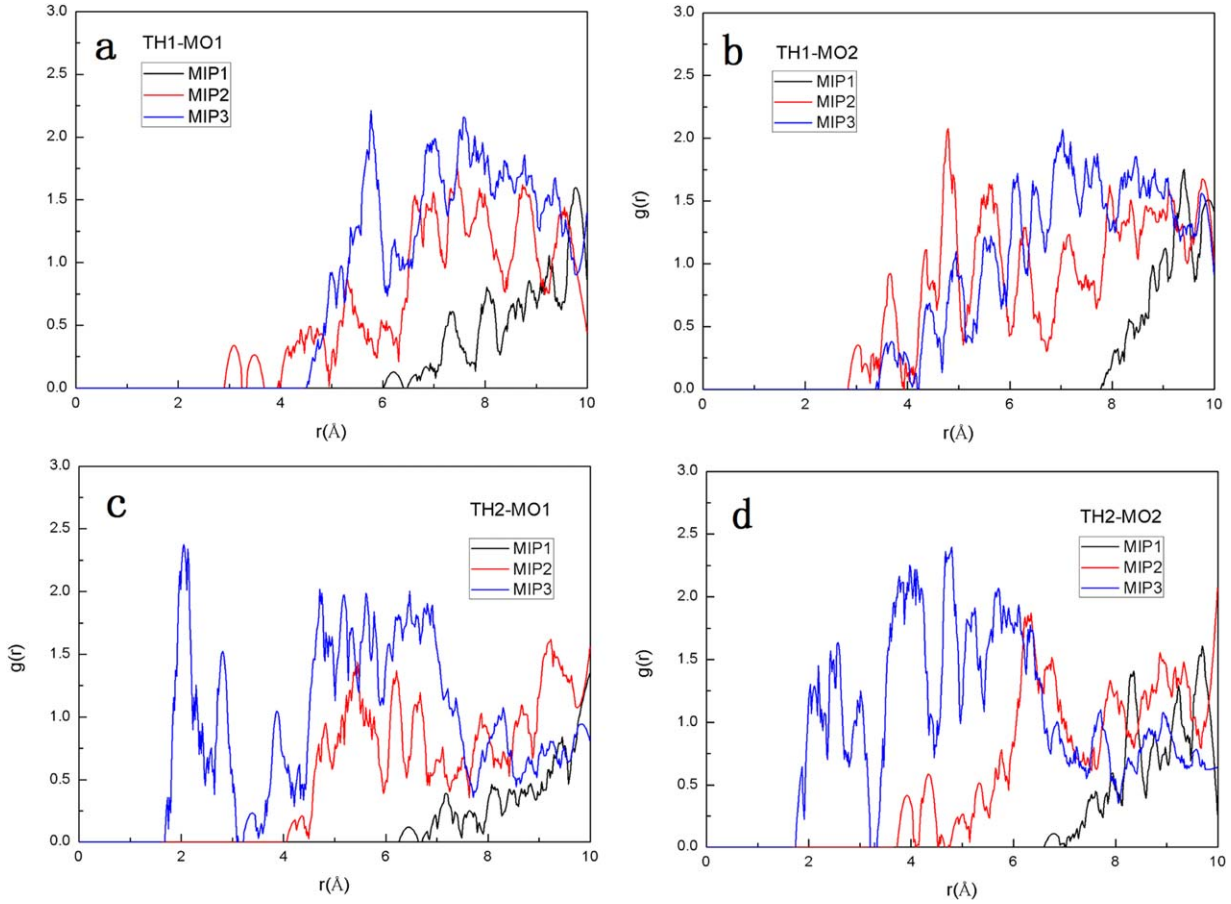

Figure 6. RDFs showing the probabilities of hydrogen atoms of NOR at different separation distances from the oxygen atom of MAA. *r* is a certain distance from a solute atom and the average bulk atom. [Color figure can be viewed in the online issue, which is available at wileyonlinelibrary.com.]

NOR, respectively; *a* represents the initial adsorption rate; and *b* is a constant related to the surface coverage.

As shown in Figure 9(a), the three kinds of MIPs had the same trend to adsorb NOR, and MIP2 had a higher adsorption capacity than MIP1 or MIP3. Increasing the size of the particles increased its adsorption ability. However, when the size was overly increased, this lowered the mass transport and adsorption efficiency. So, the adsorption capacity did not continue to increase, and MIP2 was chosen as the best one. As shown in Figure 9(a), we found that the adsorption kinetics of the MIPs were divided into three stages. In the first 60 min, a rapid increase was observed, and the phenomenon indicated that NOR was delivered from the solution to the surface of the MIPs by hydrophobic interaction. The rate between 60 and 180 min became lower because of the difficulty of osmosis. This was because the empty imprinting sites became fewer and because of the

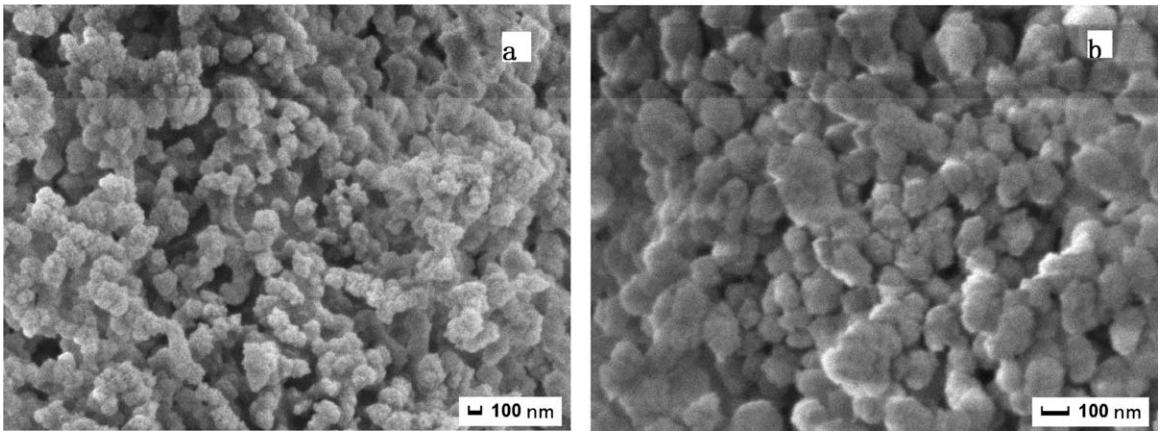

Figure 7. Scanning electron microscopy images of (a) MIP2 and (b) NIP2.

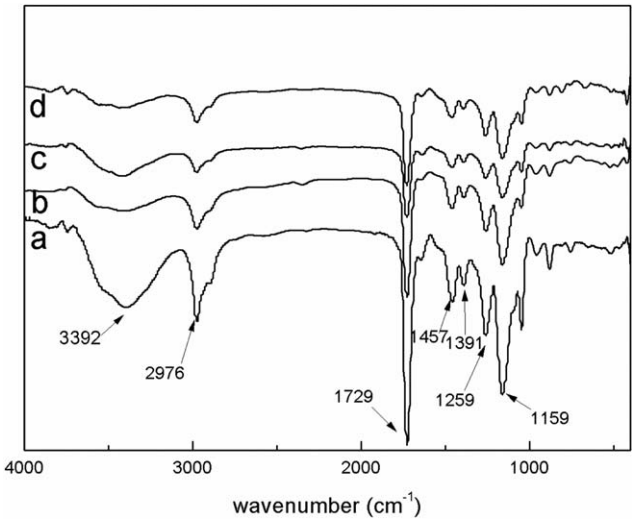

Figure 8. Fourier transform infrared spectra of (a) MIP2, (b) MIP3, (c) MIP1, and (d) NIP2.

diminution concentration difference between the solution and the imprinting shell. After 180 min, the slope was approximately zero and reached equilibrium. The adsorption capacity of MIP2 reached a value of 29.35 mg/g; this was higher than those of reported MIPs.[18,26] The trend of the NIPs was similar to that of the MIPs, except in the second stage. Because the surface of the NIPs did not have imprinting sites that could match with NOR, the adsorption capacities of the NIPs were lower than those of the MIPs, as is obvious in Figure 9. Furthermore, with the lack of imprinting sites, the osmosis in the NIPs was unapparent.

As shown in Table S1 (see the Supporting Information), in a comparison of the experimental and fitting data of the MIPs toward NOR, pseudo–second-order kinetic model was the most suitable for the experimental data, and the correlation coefficient (R^2) was closest to 1. So, we speculated that chemical adsorption was the main adsorption during the process. Similarly, the pseudo–first-order kinetic model adsorption was the best fit for the adsorption behavior of the NIPs. The increase in the level of adsorption saturation led to a decreasing adsorption rate.

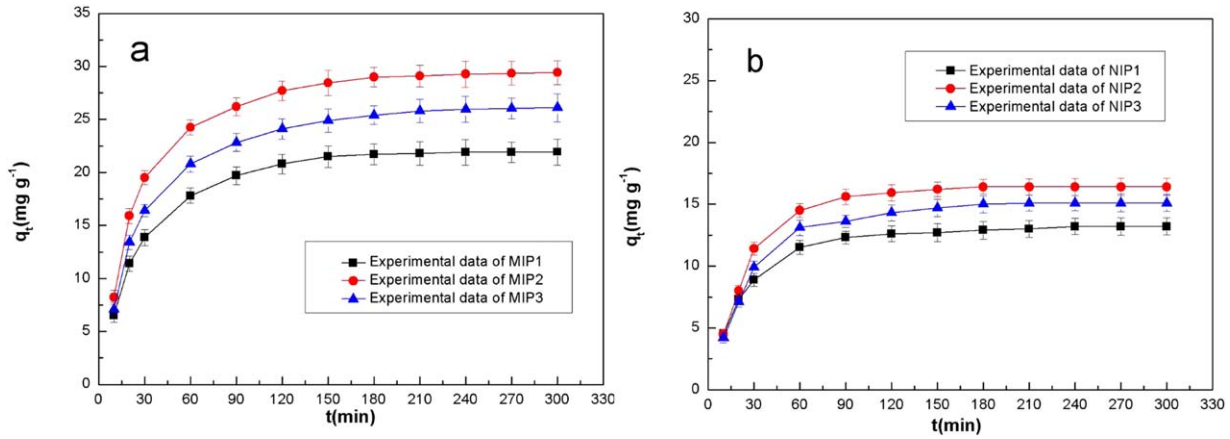

Figure 9. Kinetic adsorption curves of the (a) NOR MIPs and (b) NIPs. [Color figure can be viewed in the online issue, which is available at wileyonlinelibrary.com.]

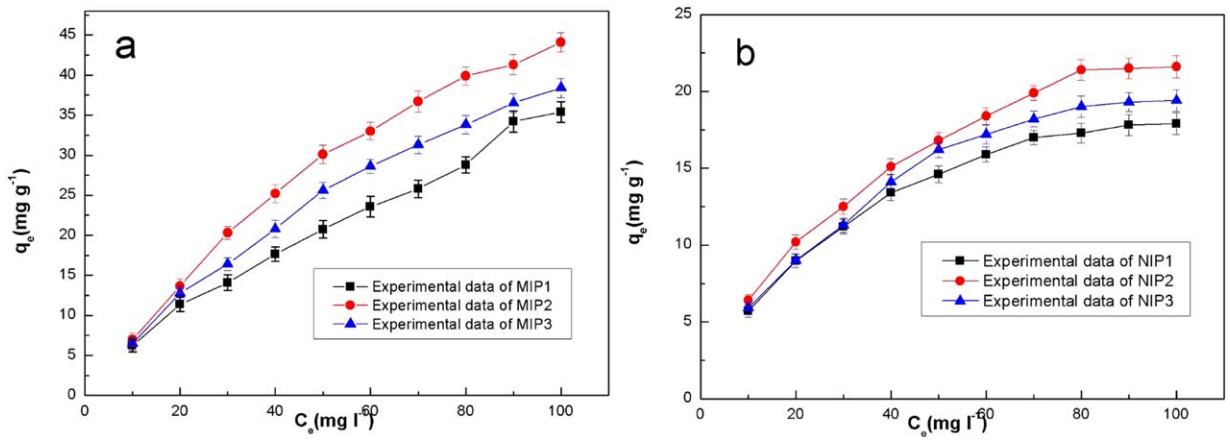

Figure 10. Adsorption isotherms curves of the NOR MIPs and NIPs. [Color figure can be viewed in the online issue, which is available at wileyonlinelibrary.com.]

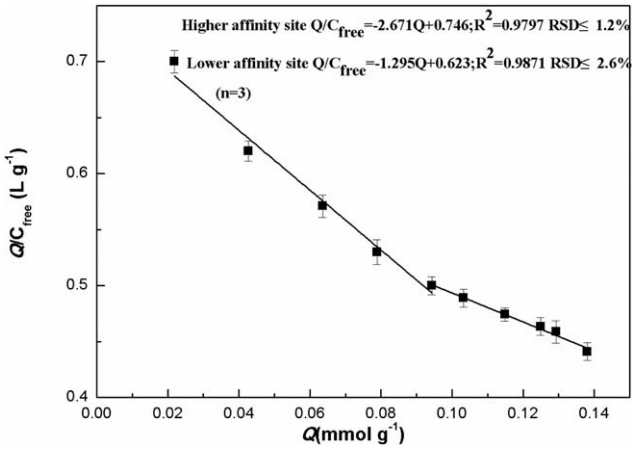

Figure 11. Adsorption isotherm and Scatchard analysis of NOR MIP2. RSD: relative standard deviation.

Analysis of the Adsorption Isotherms

In this study, the adsorption performance of the MIPs was analyzed with two-parameter isotherm models, including the Langmuir [eq. (9)] and Freundlich [eq. (10)] isothermal equations.[39,40] The parameters of the fitting adsorption isotherm are listed in Table S2 (see the Supporting Information), and the fitting nonlinear regression curves are shown in Figure 10:

$$q_e = q_{mL} k_L C_e / (1 + k_L C_e) \tag{9}$$

$$q_e = k_F C_e^{(1/nF)} \tag{10}$$

where q_{mL} is the maximum adsorption amount of monolayer adsorption, k_L is the Langmuir constant, k_F is a constant that represents the adsorption capacity, and n_F is a constant of adsorption equilibrium.

The data of the static absorption experiment were further processed according to Scatchard [eq. (11)] analysis[41] to estimate the binding parameters of MIP2:

$$\frac{Q}{C_{\text{free}}} = \frac{Q_{\max} - Q}{k_D} \tag{11}$$

where Q is the amount of NOR bound to MIP2 at equilibrium, C_{free} is the equilibrium concentration of NOR, $Q_{\max}$ is the maximum binding capacity, and K_D is the dissociation constant.

In a previous study,[34] these isotherm models were preferably interpreted as the adsorption process of the FQs on the imprinted polymers. As shown in Figure 10, the adsorption amount to NOR of the MIPs increased with increasing concentration of NOR. Meanwhile, the adsorption amount of the NIPs that grew more slowly was due to the absence of imprinting sites. The adsorption process was mainly attributed to the physical adsorption. The MIPs showed a superior adsorption performance compared to the NIPs. Under the same conditions, the absorption capacity of the MIPs was much higher than that of the NIPs, and this indicated that the MIPs had a significant adsorption effect because of the imprinting sites. Additionally, MIP2 had the best adsorption performance among these three, and the reason was similar to that previously discussed in the analysis of the adsorption kinetics. As shown in Table S2 (see the Supporting Information), the Langmuir fitting model was more suitable for the experimental data of the MIPs. This

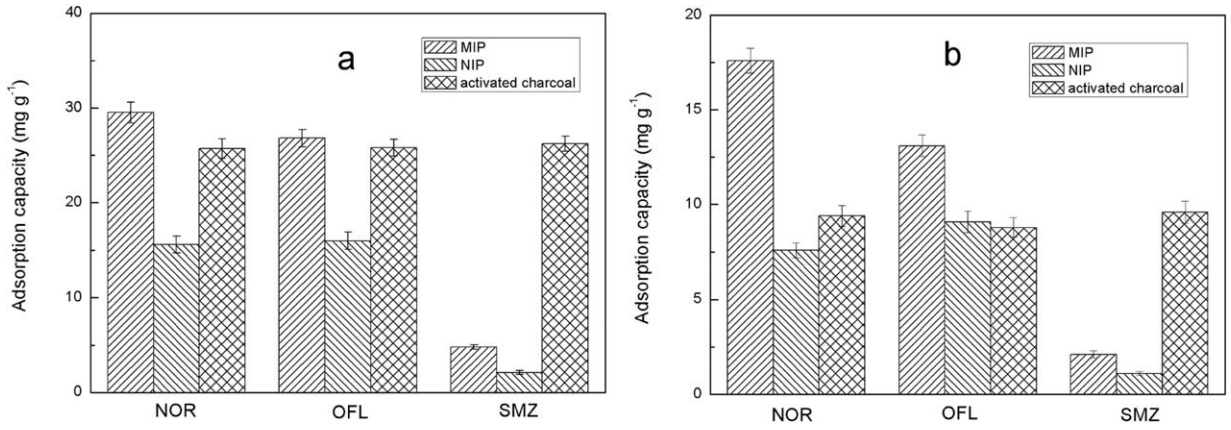

Figure 12. Adsorption capacity of different compounds on MIP2, NIP2, and activated charcoal. The solutions contained NOR, OFL, and SMZ, respectively.

Table III. Selective Recognition Parameters of MIP2 and NIP2 in Mixed Solutions

	NOR MIP2		NIP2		
Mixed solution	K_d	k	K_d	k	k'
NOR	0.7245	—	0.1942	—	—
OFL	0.4187	1.730	0.2460	0.789	2.193
SMZ	0.0447	16.208	0.0277	7.011	2.312

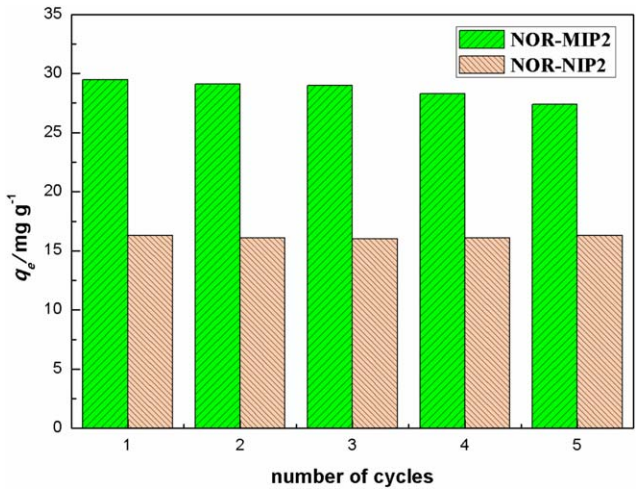

Figure 13. Reusability of the MIP2 and NIP2 particles in the NOR solution. [Color figure can be viewed in the online issue, which is available at wileyonlinelibrary.com.]

proved that the monolayer adsorption between the MIPs and NOR resulted from the hydrogen bonds and electrostatic interactions between NOR and the specific binding sites on the surfaces of the MIPs. For the NIPs, the adsorption capacity increased slowly because the adsorption behavior was multilayer.

As shown in Figure 11, the Scatchard curve was set up to according to the experimental results of MIP2. The two distinct sections within the plot could be regarded as straight lines; this indicated that two kinds of adsorption sites existed in MIP2. One had a higher adsorption capacity, and the corresponding K_{D1} and Q_{max1} values were 0.374 mmol/L and 0.279 mmol/g, respectively. The other had low a adsorption capacity, and the K_{D2} and Q_{max2} values were 0.772 mmol/L and 0.481 mmol/g, respectively.

Selectivity and Competitive Adsorption

The specific selectivity of MIP2 was evaluated by the following experiments, and the results are shown in Figure 12 and Table III. As shown in Figure 12(a), the adsorption capacity of MIP2 toward NOR was higher than those toward OFL and SMZ. More accurately, the adsorption amount of NOR was slightly higher than that of OFL and much higher than that of SMZ. We interpreted this to mean that the molecular structure of OFL was similar to that of NOR. However, compared to SMZ, the structure was quite different. The adsorption capacity of MIP2 to NOR was about eight times more than that to SMZ. What is more, although the activated carbon had high adsorption capacities toward NOR, OFL, and SMZ, the selectivity was not clear. As shown in Figure 12(b), the solution was mixed with NOR, OFL, and SMZ (50 mg/L each). From this, we could see that the adsorption capacity of activated charcoal toward all of the mixtures was equal. Compared with that toward activated charcoal, the adsorption capacities of MIP2 toward them were different.

In addition, as shown in Figure 12, the adsorption amount was less in the mixed solution than in the pure solution. The possible reason was that the imprinting sites in MIP2 interacted with both NOR and OFL. In the mixture, the total adsorption amount of MIP2 toward NOR and OFL was nearly equal to the amount of NOR in the simple NOR solution. Relative to NIP2, it displayed a lower adsorption capacity than MIP2 but a higher capacity for NOR and OFL than for SMZ. This was probably because the NOR combined with the functional monomer MAA in NIP2. As listed in Table III, in the mixed solution, K_d and k of MIP2 were higher than those of NIP2. Also, k' indicated that the adsorption capacity of MIP2 was better than that of NIP2.

In a word, MIP2 had a specific recognition ability toward NOR because of hydrogen-bonding interactions, including physical adsorption. Compared with other studies,[23,29,36] the binding selectivity of MIP toward NOR was significantly enhanced.

Regeneration of MIP2

To study the recyclability of NOR MIP2, cycling experiments were carried out at a concentration of 50 mg/L NOR. The process of adsorption was similar to the adsorption isotherms experiment. With the experiment repeated five times and the selection of the mixture of methanol and acetic acid (9 : 1 v/v) as an eluent,[42] the results are shown in Figure 13. The adsorption capacity of MIP2 lost only 7.12% after five cycles, whereas the adsorption capacity of NIP2 remained unchanged. That could have been because the imprinting sites were changed in the process of repeated washing. However, because the imprinting sites did not exist in the NIP, this indicated that the recyclability of MIP2 was favorable.

CONCLUSIONS

We designed and synthesized molecularly imprinted materials to absorb NOR specifically with a method that combined MD simulations and experimental preparation. As shown by the results, MIPs prepared with NOR as a template, MAA as a functional monomer, and EGDMA as a crosslinker at a ratio of 1 : 8 : 40 showed a high adsorption capacity (29.35 mg/g) and a short equilibrium time (120 min). Furthermore, the regeneration and selective adsorption of NOR were excellent even after five cycles. In conclusion, the MIPs designed by MD simulations were available and could be applied to practice, such as in the separation and detection of FQs.

ACKNOWLEDGMENTS

This work was subsidized by the National Natural Science Fund (contract grant number 21106056), the Jiangsu Natural Science Fund of China (contract grant number BK20141287), the Postdoctoral Science Foundation of China (contract grant number 2014M560405), the Postdoctoral Science Foundation of Jiangsu Province (contract grant number 1401012A), the Scientific Research Foundation of Jiangsu University (contract grant numbers 13A582 and 12A272), the Senior Talent Foundation of Jiangsu University (contract grant number 14JDG057), and the Zhenjiang Social Development Fund of Jiangsu Province (contract grant number SH2014020).

REFERENCES

1. Zheng, M. M.; Gong, R.; Zhao, X.; Feng, Y. Q. *J. Chromatogr. A* **2010**, *1217*, 2075.
2. Leivo, J.; Lamminmaki, U.; Lovgren, T.; Vehniainen, M. *J. Agric. Food Chem.* **2013**, *61*, 11981.

3. Chen, B. W.; Yang, Y.; Liang, X. M.; Yu, K.; Zhang, T.; Li, X. D. *Environ. Sci. Technol.* **2013**, *47*, 12753.
4. Singh, R. P.; Sastry, K. V. H.; Dubey, P. K.; Agrawal, R.; Singh, R.; Pandey, N. K.; Mohan, J. *Environ. Toxicol. Chem.* **2013**, *32*, 2134.
5. Ram, S.; Vajpayee, P.; Tripathi, U.; Singh, R. L.; Seth, P. K.; Shanker, R. J. *Pure. Appl. Microbiol.* **2008**, *105*, 1899.
6. Fung-Tomc, J. C.; Minassian, B.; Kolek, B.; Huczko, E.; Aleksunes, L.; Stickle, T.; Washo, T.; Gradelski, E.; Valera, L.; Bonner, D. P. *Antimicrob. Agents. Chemother.* **2000**, *44*, 3351.
7. Niyogi, S. K. *Clin. Microbiol. Infect.* **2007**, *13*, 1141.
8. Yan, H.; Qiao, F.; Row, K. H. *Anal. Chem.* **2007**, *79*, 8242.
9. Lulinski, P.; Maciejewska, D.; Bamburowicz-Klimkowska, M.; Szutowski, M. *Molecules* **2007**, *12*, 2434.
10. Seifrtová, M.; Nováková, L.; Lino, C.; Pena, A.; Solich, P. *Anal. Chim. Acta* **2009**, *649*, 158.
11. Zhang, M.; Huang, J.; Yu, P.; Chen, X. *Talanta* **2010**, *81*, 162.
12. Liu, X.; Guan, Y.-P.; Wang, Q.; Ren, X. F.; Yang, M. Z. *J. Appl. Polym. Sci.* **2012**, *126*, 1956.
13. Tokonami, S.; Shiigi, H.; Nagaoka, T. *Anal. Chim. Acta* **2009**, *641*, 7.
14. Sun, H. W.; Qiao, E. X. *J. Chromatogr. A* **2008**, *1212*, 1.
15. Lasáková, M.; Jandera, P. *J. Sep. Sci.* **2009**, *32*, 799.
16. Zhang, F. F.; Gu, S. Q.; Ding, Y.-P. *Anal. Chim. Acta* **2013**, *770*, 53.
17. Turiel, E.; Martin-Esteban, A.; Tadeo, J. L. *J. Chromatogr. A* **2007**, *1172*, 97.
18. Wang, J. P.; Pan, M.-F.; Fang, G. Z.; Wang, S. *Microchim. Acta* **2009**, *166*, 295.
19. Liu, S. T.; Yan, H. Y.; Wang, M. Y.; Wang, L. H. *J. Agric. Food Chem.* **2013**, *61*, 11974.
20. Zhang, D.; Lv, Y. K.; Chen, R. *Asian J. Chem.* **2013**, *25*, 3922.
21. Lv, Y. K.; Wang, L. M.; Yang, L. *J. Chromatogr. A* **2012**, *1227*, 48.
22. He, H. B.; Dong, C.; Li, B.; Dong, J.-P.; Wang, T. L.; Yu, Q. W.; Feng, Y. Q. *J. Chromatogr. A* **2014**, *1361*, 23.
23. Sun, X. L.; He, J.; Cai, G. R. *J. Sep. Sci.* **2010**, *33*, 3786.
24. Sun, X. L.; Wang, J. C.; Li, Y.; Yang, J.-J.; Jin, J.; Sha, S. Z.; Chen, J. P. *J. Chromatogr. A* **2014**, *1359*, 1.
25. Proeto, A.; Schrader, S.; Bauer, C. *Anal. Chim. Acta* **2011**, *685*, 146.
26. Caro, E.; Marcé, R. M.; Cormack, P. A. G.; Sherrington, D. C.; Borrull, F. *Anal. Chim. Acta* **2006**, *562*, 145.
27. Ghasemzadeh, N.; Nyberg, F.; Hjerten, S. J. *Sep. Sci.* **2008**, *31*, 3945.
28. Nicholls, I. A.; Andersson, H. S.; Charlton, C. *Biosens. Bioelectron.* **2009**, *25*, 543.
29. Henthorn, D. B.; Peppas, N. A. *Ind. Eng. Chem. Res.* **2007**, *46*, 6084.
30. Levi, L.; Srebnik, S. *J. Phys. Chem. B* **2010**, *114*, 107.
31. Krupadam, R. J.; Patel, G. P.; Balasubramanian, R. *Environ. Sci. Pollut. Res.* **2012**, *19*, 1841.
32. Cleland, D.; Olsson, G. D.; Karlsson, B. C. G.; Nicholls, I. A.; McCluskey, A. *Org. Biomol. Chem.* **2014**, *12*, 844.
33. Azenha, M.; Szefczyf, B.; Loureiro, D.; Kathirvel, P.; Cordeiro, M. N. D. S.; Silva, A. F. *Langmuir* **2013**, *29*, 2024.
34. Pu, X.; Dudal, Y.; Corvini, P. F.-X.; Spahr, P.; Shahgaldian, P. *React. Funct. Polym.* **2012**, *72*, 287.
35. Karlsson, B. C. G.; O'Mahony, J.; Karlsson, J. G.; Bengtsson, H.; Eriksson, L. A.; Nicholls, I. A. *J. Am. Chem. Soc.* **2009**, *131*, 13297.
36. Tang, W. J.; Zhao, T.; Zhou, C. H.; Guan, X. J.; Zhang, H. X. *Anal. Method* **2014**, *6*, 3309.
37. Castro, E. A.; Ibanez, F.; Santos, J. G. *J. Org. Chem.* **1992**, *57*, 7024.
38. Akpa, O. M.; Unuabonah, E. I. *Desalination* **2011**, *272*, 20.
39. Ebara, Y.; Okahata, Y. *J. Am. Chem. Soc.* **1994**, *116*, 11209.
40. Mbui, D. N.; Shiundu, P. M.; Ndonye, R. M. *J. Environ. Monitor.* **2002**, *4*, 978.
41. Yan, H.; Qiao, F.; Row, K.-H. *Anal. Chem.* **2007**, *79*, 8242.
42. Cao, Y.; Liu, L. K.; Xu, W. Z.; Wu, X. Y.; Huang, W. H. J. *Appl. Polym. Sci.* **2013**, *131*, 40473.